Nano Research
2022, 15(8): 7313–7319

ISSN 1998-0124 CN 11-5974/O4
https://doi.org/10.1007/s12274-022-4351-1

Research Article

Sensitively detecting antigen of SARS-CoV-2 by NIR-II fluorescent nanoparticles

Ruibin Hu[1,§], Tao Liao[2,§], Yan Ren[3,§], Wenming Liu[2], Rui Ma[1], Xinyuan Wang[1], Qihui Lin[3] (✉), Guoxin Wang[2] (✉), and Yongye Liang[1] (✉)

[1] *Department of Materials Science and Engineering, Southern University of Science and Technology of China, Shenzhen 518055, China*
[2] *WWHS Biotech. Inc., Shenzhen 518122, China*
[3] *Joint Laboratory for Infectious Disease Prevention and Control, Hygienic Section of Longhua Center for Disease Control and Prevention, Longhua District, Shenzhen 518109, China*
[§] *Ruibin Hu, Tao Liao, and Yan Ren contributed equally to this work.*

Received: 6 February 2022 / **Revised:** 19 March 2022 / **Accepted:** 22 March 2022

ABSTRACT

Early detection of severe acute respiratory syndrome coronavirus 2 (SARS-CoV-2) infection is an efficient way to prevent the spread of coronavirus disease 2019 (COVID-19). Detecting SARS-CoV-2 antigen can be rapid and convenient, but it is still challenging to develop highly sensitive methods for effective diagnosis. Herein, a lateral flow assay (LFA) based on fluorescent nanoparticles emitting in the second near-infrared (NIR-II) window is developed for sensitive detection of SARS-CoV-2 antigen. Benefiting from the NIR-II fluorescence with high penetration and low autofluorescence, such NIR-II based LFA allows enhanced signal-to-background ratio, and the limit of detection is down to 0.01 ng·mL^{-1} of SARS-CoV-2 antigen. In the clinical swab sample tests, the NIR-II LFA outperforms the colloidal gold LFA with higher overall percent agreement with the polymerase chain reaction test. The clinical samples with low antigen concentrations (~ 0.015–~ 0.068 ng·mL^{-1}) can be successfully detected by the NIR-II LFA, but fail for the colloidal gold LFA. The NIR-II LFA can provide a promising platform for highly sensitive, rapid, and cost-effective method for early diagnosis and mass screening of SARS-CoV-2 infection.

KEYWORDS

coronavirus disease 2019 (COVID-19), severe acute respiratory syndrome coronavirus 2 (SARS-CoV-2), antigen detection, the second near-infrared (NIR-II) fluorophores, lateral flow assay

1 Introduction

Severe acute respiratory syndrome coronavirus 2 (SARS-CoV-2), identified as the causative agent of the coronavirus disease 2019 (COVID-19) [1, 2], has caused a worldwide pandemic and posed a huge challenge for global public health. By February 2022, the number of patients with SARS-CoV-2 pneumonia reaches 380 million and the death toll exceeds 5 million [3]. The data still increase every day. The direct human to human transmission, the indefinite incubation period of carriers, and the nonspecific symptoms of carriers are the main reasons for such high infectivity of SARS-CoV-2 [4, 5]. To prevent transmission and control pandemic of COVID-19, it is necessary to exploit advanced methods to detect it in the early stage of infection.

Up to now, researchers have developed numerous early diagnostic kits, which can be divided into two categories: genetic material-based molecular diagnosis or antigen/antibody-based immunoassays. For nucleic acid quantification analysis, quantitative reverse transcription polymerase chain reaction (qRT-PCR) is regarded as the gold standard for COVID-19 detection because of its mature technique and high sensitivity [6, 7]. However, it requires specific equipment and laboratory, which is apparently not suitable for rapidly detecting the virus in point of care (POC) setting.

Immune-based assays are based on the high affinity between antigen and antibody, affording high specificity and rapid response (about a few minutes) [8], and they are very suitable for rapid diagnosis of COVID-19. These methods mainly include enzyme-linked immunosorbent assays (ELISA) [9–11], chemiluminescent immunoassays (CLIA) [12–14], and lateral flow assays (LFA) [15–17]. LFA technique is advantageous for its simplicity, convenience, rapidity, and cost-efficiency. As early as February 2020, SARS-CoV-2 antibody detection kit was developed [18]. So far, a variety of SARS-CoV-2 antibody assay kits based on colloidal gold LFA have been widely used [19–21]. However, the antibody test cannot be used alone as a diagnostic indicator for screening of SARS-CoV-2 infection as it generally takes more than 7 days for the body to produce antibodies after infection [22–24]. In this window period, the viral load increased rapidly along with the acceleration of reproduction and the infection risk increases further [25, 26]. In contrast, antigen can be detected at the earlier stage of infection. Rapid antigen detection by LFA has been developed for case finding and contract tracing of COVID-19 [27]. However, the concentration of virus contained in the sampling could be low as it is generally acquired from the upper respiratory tract, but COVID-19 mainly infringes on the lower respiratory tract areas. In this situation, highly sensitive viral

Address correspondence to Yongye Liang, liangyy@sustech.edu.cn; Guoxin Wang, wanggx@wwhsbio.com; Qihui Lin, lhjkzx@szlhq.gov.cn

antigen detection technique is urgently required.

In the past two years, improved antigen detection methods of SARS-CoV-2 have been reported [28–31]. For instance, Guo et al. developed an up-conversion nanoparticles based LFA for quantitative detection of spike (S) protein and nucleocapsid (N) protein of SARS-CoV-2. In this platform, the sensor could detect the S protein and N protein with limit of detection (LoD) of 1.6 and 2.2 ng·mL^{-1}, respectively [32]. Grant et al. demonstrated a half-strip LFA for detection of N protein, achieving a LoD of 0.65 ng·mL^{-1} with an optical reader [33]. Liu et al., reported a nanozyme-based test with the lateral flow strip. Co-Fe@hemin-peroxidase nanozymes were constructed for catalyzing chemiluminescence similar with the natural horseradish peroxidase (HRP), leading to the amplification of the detection signals. And the LoD is improved to 0.1 ng·mL^{-1} [34]. However, the determination of clinical samples with lower concentration viruses is still challenging. Thus, a robust analytical technology with higher sensitivity is urgently needed.

Recently, fluorophores emitting in the second near-infrared (NIR-II) window with wavelengths ranging from 1,000 to 1,700 nm have achieved visualization of deep anatomical features in *in vivo* biological imaging [35–39]. Compared with the visible and the first near infrared window (NIR-I, ~ 700–1,000 nm), the imaging in the NIR-II window can reduce scattering and absorption of photons and lower background auto-fluorescence, affording improved signal to background ratio (SBR) [40, 41]. The coupling of NIR-II fluorescent dyes with biomarkers of SARS-CoV-2 may offer improved visualization modality to understand virus function *in vivo*. In another side, these features are also favored for detection of biological *in vitro* assays. However, NIR-II fluorescence has been rarely explored for biological *in vitro* assay application.

In this study, we applied the NIR-II fluorescent nanoparticles for LFA, and demonstrated sensitive detection of SARS-CoV-2 antigen. The sample concentration was analyzed by the fluorescent signal of over 1,000 nm from the NIR-II fluorescent nanoparticles, affording low background interference and high sensitivity. LoD of 0.01 ng·mL^{-1} and a wide analytical range of 0.02–120 ng·mL^{-1} were achieved for N protein of SARS-CoV-2. In a preliminary measurement of 30 clinical pharyngeal swabs (18 COVID-19 infected and 12 uninfected), the NIR-II LFA could successfully detect all the positive samples due to the enhanced SBR. In contrast, the colloidal gold LFA failed to detect 10 positive samples with viral load below ~ 0.068 ng·mL^{-1}.

2 Results and discussion

2.1 Characterization of NIR-II nanoparticles

The NIR-II fluorescent nanoparticles were prepared by encapsulating organic dyes in polystyrene (PS) nanoparticles (obtained from WWHS Biotech, Inc.). The nanoparticle surface was modified with carboxyl groups, allowing conjugation with the amine functionalized monoclonal antibodies (mAbs117). Scanning electron microscopy (SEM) images showed the nanoparticle size increased and the surface became rough after conjugating with mAbs117 (Fig. 1(a)). The dynamic light scattering (DLS) measurement indicated that the mean diameter of the NIR-II nanoparticles was 295.3 ± 5 nm. The size of the labeled NIR-II nanoparticles increased by 47 nm, reaching 342.0 ± 1.3 nm (Fig. S1 in the Electronic Supplementary Material (ESM)), suggesting that the antibodies were successfully conjugated to the surface of NIR-II nanoparticles. The aqueous dispersion of the nanoparticles was light green, and showed bright NIR-II fluorescence (Fig. 1(b)). The ultraviolet–visible–NIR (UV–Vis–NIR) absorption spectrum of the NIR-II nanoparticles displayed a peak at 806 nm, whereas the fluorescence emission was peaked at 1,046 nm (Fig. 1(c)).

2.2 Principle of the NIR-II LFA for detecting SARS-CoV-2 antigen

NIR-II fluorescent nanoparticles were introduced to design a rapid LFA for SARS-CoV-2 diagnosis (Fig. 2). The LFA strip consisted of five parts, sample pad, conjugation pad, nitrocellulose (NC) membrane, absorbent pad, and plastic backing. The as-prepared antibody labeled nanoparticles (NIR-II nanoparticles@mAbs117) were immobilized on conjugation pad. And the N protein capture antibodies (mAbs30) and streptavidin were dispensed on the test line (T line) and control line (C line) on the NC membrane respectively, and the gap between the T and C lines was ~ 3 mm. After being loaded onto the sample pad, sample liquid flowed along the strip to the absorbent pad by capillary forces. During the flowing, the mAbs117 labeled nanoparticles@SARS-CoV-2 N protein complexes formed on the conjugation pad were captured by the mAbs30 antibodies at the T line via the antigen–antibody interaction between SARS-CoV-2 N protein and mAbs30, forming a sandwich immune-complexes structure. The more N proteins in the sample, the more sandwich immune-complexes were aggregated at test line. As the liquid continued to flow, the

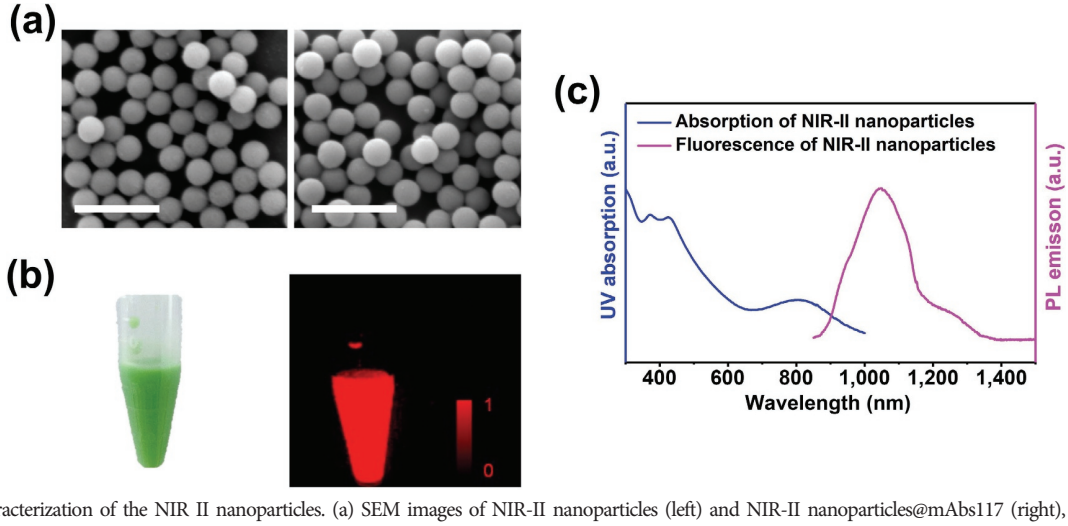

Figure 1 Characterization of the NIR II nanoparticles. (a) SEM images of NIR-II nanoparticles (left) and NIR-II nanoparticles@mAbs117 (right), the scale bar is 1 μm. (b) The optical and florescent images of the NIR-II nanoparticle dispersion in water. (c) The absorption and fluorescence spectra of the NIR-II nanoparticle dispersion in water.

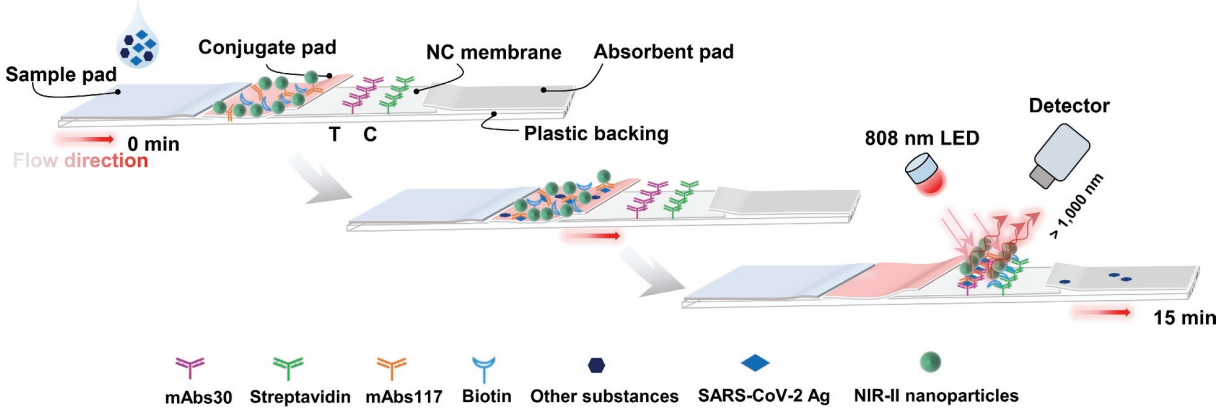

Figure 2 NIR-II lateral flow assay for detection of SARS-CoV-2 antigen. T: test line; C: control line. In the presence of SARS-CoV-2 N protein, a sandwich complex with NIR-II nanoparticles would be formed on the test line. Without the N protein, only NIR-II nanoparticles@biotin would be bound to streptavidin on the control line.

NIR-II nanoparticles labeled with biotin were trapped by the streptavidin at C line. An 808 nm light-emitting diode was employed to excite the NIR-II nanoparticles and the fluorescent signals were recorded by a low-cost InGaAs photodetector operated at room temperature after filtering with a 1,000 nm long-pass filter (Fig. S2(a) in the ESM). And the fluorescent signal was positively correlated with the number of the fluorescent nanoparticles. Quantitative sample concentration could be obtained by establishing the corresponding relationship between antigen concentration and fluorescent intensity through integrating the fluorescent signal intensity at the T and C lines (Fig. S2(b) in the ESM). Based on this principle, a highly sensitive SARS-CoV-2 antigen lateral flow assay method was developed, which could be applied to the SARS-CoV-2 early diagnosis by quantifying its antigen.

2.3 Quantitative analysis of the NIR-II LFA

The optimized antibody loading on NIR-II nanoparticles and immunoassay time were first screened. It showed that the T/C signal intensity gradually increased with the antibody concentration up to 240 ng·mL^{-1}. Then the T/C signal intensity did not change significantly when the antibodies concentration ranged from 240 to 360 ng·mL^{-1} (Fig. S3(a) in the ESM). The immunoassay time was also investigated, and the result indicated that the T/C signal intensity increased rapidly in the first 15 min, then tended to be saturated after 15 min (Fig. S3(b) in the ESM). Thus, the antibodies concentration of 240 ng·mL^{-1} and immunoassay time of 15 min were chosen for later studies.

Subsequently, the sensitivity of the NIR-II based LFA was evaluated by detecting SARS-CoV-2 recombinant antigen with varying concentration. The SARS-CoV-2 N protein solutions (100 μL) with the concentration range of 0 to 120 ng·mL^{-1} were loaded onto the sample pad, respectively. With the increase of N protein concentration, the T/C signal intensity increased accordingly (Fig. 3(a)). There was a good linearity relationship between the T/C intensity and the concentration of N protein in the range of 0.02–120 ng·mL^{-1}, and the correlation coefficient (R^2) was over 0.99. Further, a series of low concentration experiments were carried out near the detection threshold. And the LoD was down to 0.01 ng·mL^{-1}, which was calculated by the mean signal intensity of blank plus triples of standard deviation (Fig. 3(b)). Other SARS-CoV-2 antigen detection methods based on LFA were then introduced to compare, and the NIR-II LFA is advantageous for its high sensitivity (Table 1).

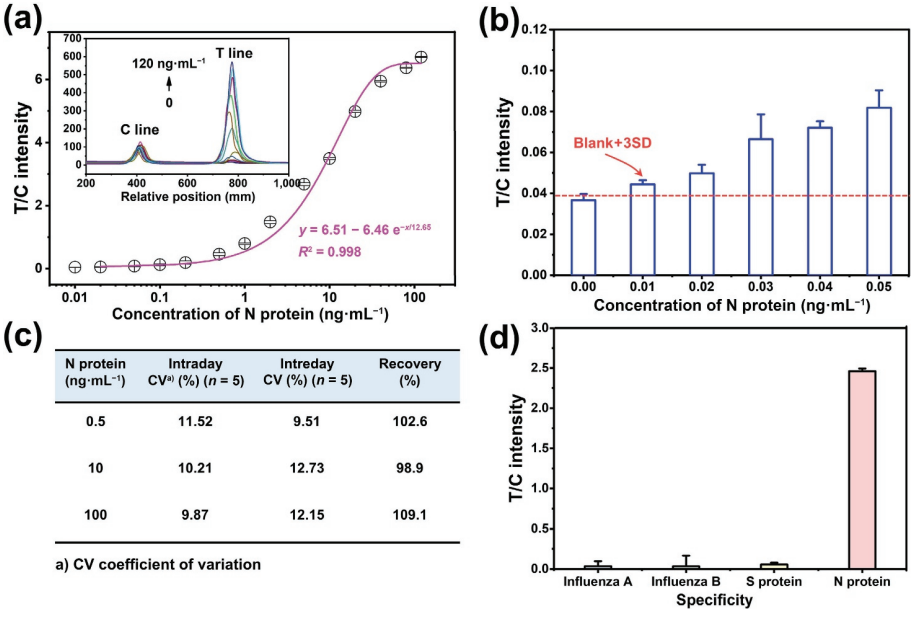

N protein (ng·mL^{-1})	Intraday CV[a] (%) (n = 5)	Intreday CV (%) (n = 5)	Recovery (%)
0.5	11.52	9.51	102.6
10	10.21	12.73	98.9
100	9.87	12.15	109.1

a) CV coefficient of variation

Figure 3 Analytical performance of the NIR-II LFA. (a) Standard curve for N protein. Inset showed the signal intensity distribution curves of various concentration of N protein. (b) Sensitivity of the NIR-II LFA. The limit of detection, was calculated by the blank intensity plus three fold standard deviation, was 0.01 ng·mL^{-1}. (c) Key parameters of NIR-II LFA. Stability and reproducibility of the NIR-II LFA. (d) Specificity of the NIR-II LFA. The concentration of influenza A, influenza B, S protein, and the target was 5 ng·mL^{-1}. All the data were obtained from over three independent measurements.

The reproducibility is a key factor in evaluating the effectiveness of a method. Herein, it was evaluated by intraday, intreday variations, and recovery rates. Coefficient of variation (CV) was below 11.6% for intraday and below 12.8% for interday. Recovery rates at N protein concentrations of 0.5, 10, and 100 ng·mL^{-1} were estimated to 102.6%, 98.9%, and 109.1%, respectively (Fig. 3(c)). We also verified the specificity of our strips by measuring the influenza A, influenza B, S protein (SARS-CoV-2 recombinant spike protein), and N protein, respectively. The results showed that our strips could specifically recognize SARS-CoV-2, and there were no cross reactions with other proteins (Fig. 3(d)). It demonstrated that our NIR-II LFA showed high specificity for SARS-CoV-2.

2.4 Performance comparison with the colloidal gold-based LFA

From the test of low antigen concentrations, it could be found that the T line was clearly distinguished from the background signal and the SBR was up to 3.46 when the antigen concentration was down to 0.1 ng·mL^{-1} (Fig. 4(a)). When the antigen concentration was as low as 0.01 ng·mL^{-1}, the SBR could still reach 1.21, though the T line looks blurred (Fig. 4(a)).

Subsequently, commercial colloidal gold-based assay kits were accessed for comparison. In the colloidal gold-based assay kits prepared with the same antibody, the T line was indistinct when the antigen concentration was diluted to 0.1 ng·mL^{-1} and SBR at 0.5 ng·mL^{-1} was only 1.23 (Fig. 4(b)). In another commercial colloidal gold-based SARS-CoV-2 antigen kits (Wandfo Biotech Co., Ltd., cat. W19610617), the T line was indistinct when the antigen concentration was diluted to 0.5 ng·mL^{-1} (Fig. S4 in the ESM). These results suggested that the NIR-II LFA was more sensitive than colloidal gold LFAs for SARS-CoV-2 antigen detection.

2.5 Preliminary application of the NIR-II LFA for clinical samples test

To further validate the NIR-II LFA, we measured 30 clinical swab samples including 18 COVID-19 positive samples and 12 COVID-19 negative samples (PCR-confirmed, from Shenzhen Center for Disease Control and Prevention, China). In NIR-II LFAs, the positive samples and negative samples could be clearly distinguished by comparing the fluorescence intensity distribution curves (Figs. S5(a) and S5(b) in the ESM) and T/C values (Fig. S5(c) in the ESM). For the tested negative samples, the T/C values were around 0.035–0.039. In the positive samples, the detected N protein concentrations derived from the T/C values were between 0.015 and 13.906 ng·mL^{-1}. Of which, 10 cases had low antigen concentrations ranging from 0.015 to 0.068 ng·mL^{-1} (Fig. 5(a)). Afterwards, we tested the performance of colloidal gold strips (WWHS Biotech, Inc.). Only 8 cases with high antigen concentrations were detected from the 18 positive samples (Fig. 5(b) and the red boxes in Fig. S6 in the ESM). The remaining 10 cases with low antigen concentrations (< 0.068 ng·mL^{-1}) could not be distinguished from the negative samples based on the established cutoff values (the purple ones showed in Fig. 5(b) and Fig. S6 in the ESM). As summarized in Fig. 5(c), the NIR-II LFA outperformed the colloidal gold LFA as it could reduce the number of false negative samples. It should be pointed that the sample preservation solution and preservation time may affect the accuracy of antigen quantification in clinical samples. Current results imply that the NIR-II method can achieve more sensitive COVID-19 determination in case of suspected cases or earlier stage of infection with lower viral loads, but more detailed study of clinical COVID-19 samples is needed for future applications.

3 Conclusions

In summary, we have reported a sensitive LFA for SARS-CoV-2 antigen detection based on NIR-II fluorescent nanoparticles

Table 1 NIR-II based lateral flow assays versus other reports on SARS-CoV-2 antigen detection

Analyte	Method	LoD	Analytical range	Ref.
N protein	The latex fluorescent microspheres-based test strip	0.1 μg·mL^{-1}	Not mentioned	[42]
N protein	N protein-specific single chain variable fragment-crystallizable fragment fusion antibodies coupling with cellulose nanobead-based LFA	20 ng ·mL^{-1}	Not mentioned	[28]
S & N proteins	Silica encapsulated up-conversion nanoparticles labeled LFA	1.6 ng·mL^{-1} for S protein; 2.2 ng·mL^{-1} for N protein	2–200 ng·mL^{-1} for both	[32]
N protein	Screening of aptamers for N protein combined with LFA	1.0 ng·mL^{-1}	Not mentioned	[30]
N protein	A half-strip LFA with carboxylic red latex beads	0.65 ng·mL^{-1}	Not mentioned	[33]
S-RBD antigen	Nanozyme and enzymatic chemiluminescence immunoassay integrate with the lateral flow strip	0.1 ng·mL^{-1}	0.2–100 ng·mL^{-1}	[34]
N protein	Fluorescent immunochromatographic assay with Cd based multilayered silica quantum dots	5.0 pg·mL^{-1}	0.01–100 ng·mL^{-1}	[43]
N protein	NIR-II fluorescent particles based LFA	0.01 ng·mL^{-1}	0.02–120 ng·mL^{-1}	This work

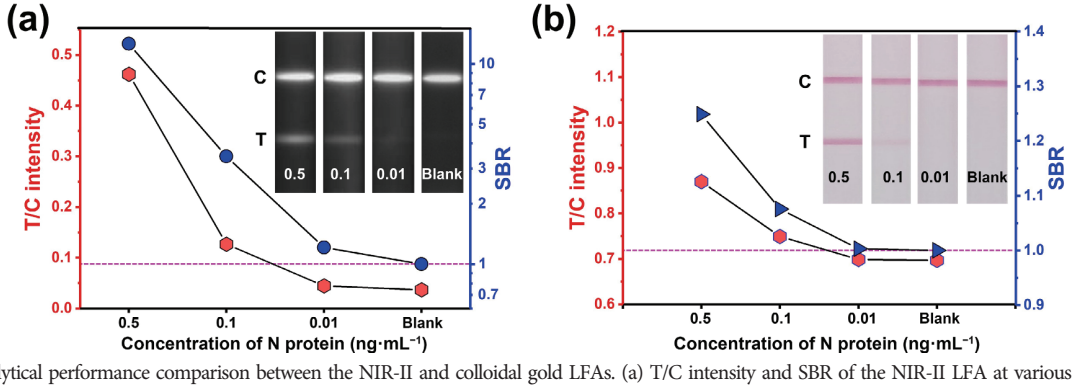

Figure 4 Analytical performance comparison between the NIR-II and colloidal gold LFAs. (a) T/C intensity and SBR of the NIR-II LFA at various concentrations recorded from the optical reader. (b) T/C intensity and SBR of the colloidal gold LFA at various concentrations (calculated from the pixel values by ImageJ software). Insets showed the optical images of the test strips.

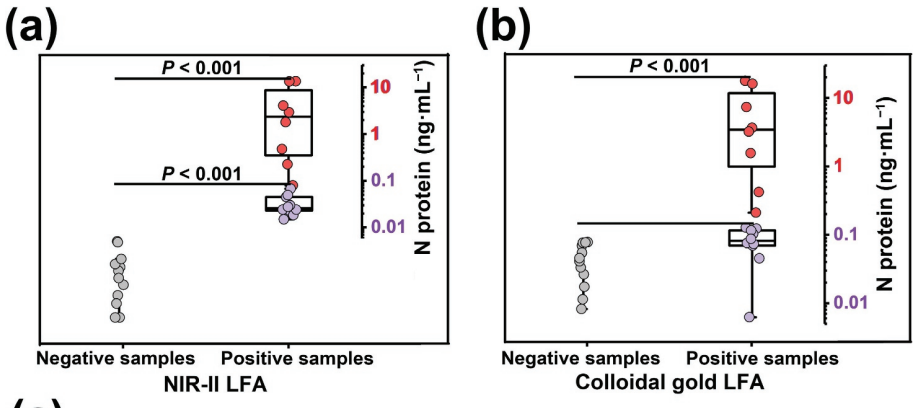

(c)

SARS-CoV-2 antigen detection					
	Positive	False positive	Negative	False negative	Total
NIR-II LFA	18	0	12	0	30
Colloidal gold LFA	8	0	12	10	30

Figure 5 Clinical swab sample detection by the NIR-II and colloidal gold LFAs. (a) Clinical swab samples detection by the NIR-II LFA. (b) Clinical swab samples detection by the colloidal gold LFA. The corresponding N protein concentration is calculated from the established fitting equation between antigen and T/C value. 10 clinical swab samples with low antigen concentration (as the purple shown) could not be distinguished from the negative swab samples by the colloidal gold LFA. Symbol legend $P < 0.001$ (significant difference, calculated by Student's *t*-test). (c) Summary of the test results of the clinical samples.

loaded with the capture antibody of N protein. A remarkable feature of the platform is that the NIR-II fluorescence detection afford higher SBR due to its advance in reducing photo scattering, light absorption, and auto-fluorescence, affording a low LoD of 0.01 ng·mL^{-1} for detecting SARS-CoV-2 antigen. Impressively, the clinical swab samples with the antigen content range from 0.015 to 0.068 ng·mL^{-1} could be successfully detected by using the NIR-II LFA, while the colloidal gold LFA failed within this concentration range. This NIR-II LFA assay enables not only rapidness but also high sensitivity, meeting the demand of early SARS-CoV-2 diagnosis with lower viral load. It should be pointed out that a low-cost InGaAs photodetector is adopted in present method, and we believe the detection sensitivity can be further increased by improving the performance of the reader. By estimating the consumables including lysis buffer and test card, the cost for each test was ca. U.S.$1.0 (Table S1 in the ESM), which was be equivalent to commercial colloidal gold LFA kits. Hence, the NIR-II LFA with cost-effectiveness, high sensitivity, and high specificity, is suitable for rapid/mass screening of COVID-19. It is also promising for point-of-care diagnosis with enhanced performances.

4 Experimental

4.1 Reagents

The NIR-II nanoparticles were provided by WWHS Biotech. Inc., (Shenzhen, China). Bovine serum albumin (BSA), biotin, streptavidin, boric acid, sodium tetraborate, 2-morpholinoethanesulfonic acid (MES), ethylenediaminetetraacetic acid disodium salt (EDTA·2Na), Tris-HCl, Tween-20, ethanolamine, 1-ethyl-3-(3-dimethytaminopropyl) carbodiimide (EDC), N-hydroxysuccinimide (NHS), and phosphate buffered saline (PBS) were obtained from Aladdin reagent (Shanghai, China). NaN_3 was purchased from Sigma Aldrich. N protein (SARS-CoV-2 Nucleocapsid-His recombinant antigen protein), S protein (SARS-CoV-2 spike recombinant antigen protein), mAbs30 (SARS-CoV-2 N protein capture antibody), and mAbs117 (SARS-CoV-2 N protein binding antibody) were purchased from FRPON Biotech Co., Ltd. (Dong guan, China). Influenza A virus antigen, influenza B virus antigen were purchased from Biocom Biotech Co., Ltd. (Nanjing, China). Fiberglass pads, absorbent pads, and PVC plastic boards were purchased from Kinbio Tech. Co., Ltd. (Shanghai, China). Nitrocellulose membrane was purchased from Nirmidas Inc., (Palo Alto, USA). Colloidal gold LFA kits were purchased from WWHS Biotech. Inc. and Wandfo Biotech Co., Ltd. Other chemicals used in this study were of analytic grade. Deionized water (≥ 18.2 MΩ·cm) purified using a Milli-Q purification system was used in all experiments.

4.2 Characterization and Instruments

The morphology of NIR-II nanoparticles, NIR-II nanoparticles labeled with antibody was analyzed by SEM (TESCAN MIRA3 LM microscope) images, and the size distribution of the NIR-II nanoparticles and NIR-II nanoparticles@mAbs117 was also characterized by DLS (Zetasizer Pro, Malvern Panalytical) measurements. All NIR-II images were taken by the DeepVision™ Imaging System (Nirmidas Biotech Inc.). All data were analyzed by origin 2017.

4.3 Conjugation between NIR-II nanoparticles and SARS-CoV-2 antibodies

200 μL 1% NIR-II nanoparticles were dispersed into 1 mL 0.1 M MES buffer (pH 6.0) by sonication. 50 μL EDC (10 mg·mL^{-1} in 0.1 M MES buffer) and 150 μL NHS (10 mg·mL^{-1} in 0.1 M MES buffer) were added to activate the carboxylic acid groups on the NIR-II nanoparticles' surface for 12 min at room temperature. After that, the activated NIR-II nanoparticles were washed with the conjugation buffer (140 mM boric acid and 15 mM sodium tetraborate, pH 6.5) three times and finally dispersed into 400 μL conjugation buffer. 48 μg mAbs117 was then added to conjugation buffer with gentle stirring for 3 h at room temperature, and the nanoparticles were coupled with antibodies by EDC/NHS agents. Then, 1 mL blocking solution (0.5% BSA, 0.1% casein in 50 mM

Tris-HCl, and pH 8.0) and 3 μL ethanolamine were added to quench and block the reaction for 2 h. Further, the nanoparticles were washed with the washing buffer (1 × PBS containing 0.5% BSA, 0.1% NaN_3, 0.4% Tween-20, and pH 7.4) for three times. And the nanoparticles were finally re-dispersed into 1 mL washing buffer. Finally, the antibody-labeled NIR-II nanoparticles were stored at 4 °C for later studies. Accordingly, the biotin-labeled NIR-II nanoparticles (NIR-II nanoparticles@biotin) were obtained by a similar procedure.

4.4 Assembing lateral flow test strips

The strip was composed of a plastic backing, a sample pad, a conjugation pad, a NC membrane and an absorption pad. The sample pad was fiberglass treated with the buffer (0.4% BSA, 1.2% Tris-HCl, 0.12% EDTA, 0.1% NaN_3, 0.4% Tween-20, and pH 8.0), and the conjugation pad was fiberglass treated with the buffer (10% trehalose, 0.5% BSA, 0.1% casein, and pH 8.0). The treated sample pad and conjugation pad were dried at 37 °C and 25% relative humidity overnight. 25 μL, mAbs30 (1.0 mg·mL^{-1}) and 25 μL streptavidin (1.0 mg·mL^{-1}) were dispensed at test and control region on the NC membrane, respectively, using a HM3030XYZ dispenser (KinbioTech Co., Ltd., Shanghai, China) at a rate of 2.25 μL·cm^{-1} and a speed of 10 cm·s^{-1} and then dried at 37 °C and 25% relative humidity overnight. 20 μL antibody-labeled NIR-II nanoparticles, 5 μL biotin-labeled NIR-II nanoparticles mixed with 2 mL conjugation pad buffer (10% trehelose, 0.5% BSA, 0.1% casein, and pH 8.0) were used to treat the conjugation pads, and dried at 37 °C and 25% relative humidity overnight. As a result, the labeled NIR-II nanoparticles were immobilized on the conjugation pads. The absorption pad, NC membrane, pretreated conjugation pad, and sample pad were attached to the plastic backing and assembled as a trip with a 1–2 mm overlap sequentially. The assembled plate was cut into pieces with a width of 3 mm, using an automatic strip cutter ZQ2000 (KinbioTech Co., Ltd., Shanghai, China). The strips were stored at room temperature and 25% relative humidity.

4.5 NIR-II based lateral flow assay for SARS-CoV-2 standard antigen

The antigen of N protein was diluted to 120, 80, 40, 20, 10, 5, 2, 1, 0.5, 0.2, 0.1, 0.05, 0.04, 0.03, 0.02, 0.01, and 0 ng·mL^{-1} successively with the dilution buffer (1 × PBS including 0.5% BSA, 0.5% Tween-20, 0.1% NaN_3, and pH 7.4), and 100 μL diluted antigen was loaded onto the sample pad of the strips. No less than three parallel measurements were carried out for each concentration. The strips were scanned after 15 min post-loading. The results were denoted as the fluorescence peak area of the T line and C line. Subsequently, the relationship between T/C value and N protein concentration was established. In addition, the stability and specificity were investigated by using the pure antigen of N protein.

4.6 The NIR-II LFA for clinical samples

Nasopharyngeal swabs from COVID-19 clinical samples (18 positive cases and 12 negative cases, confirmed by qRT-PCR) were stored in a universal transport medium. In the process, the viruses were inactivated in the preservation solution and then stored at −80 °C for later use. The experiment was carried out as follows: 100 μL diluted swabs were loaded onto the sample pad of the strip. And the strip was scanned after 15 min post-loading. The signal was collected by the optical reader. In addition, the performance of colloidal gold strips (WWHS Biotech, Inc.) was evaluated by testing these clinical samples. All tests were conducted in a standard P2 laboratory by trained personnel, avoiding potential safety risks.

Acknowledgements

This work is supported by Guangdong Provincial Department of Science and Technology-key research and development project (No. 2020B1111160003), Shenzhen Science and Technology Innovation Commission technology breakthrough project (No. JSGG20191231141403880), Shenzhen San-Ming Project (No. SZSM201809085), and Shenzhen Science and Technology Innovation Commission general project (No. JCYJ20180504165657443). Also, we are grateful to the Shenzhen Center for Disease Control and Prevention for providing and detecting the clinical samples.

Electronic Supplementary Material: Supplementary material (the operation procedure and cost of the materials needed of NIR-II lateral flow assays, the dynamic light scattering spectrum of the NIR-II nanoparticles, the components and testing principle, optimization of main parameters pertaining to the LFA performance, the colloidal gold LFA strip, the fluorescence intensity distribution curves and the T/C values of the strips for clinical samples by NIR-II LFA, and results of clinical swab samples detected by colloidal gold LFA) is available in the online version of this article at https://doi.org/10.1007/s12274-022-4351-1.

References

[1] Wang, C.; Horby, P. W.; Hayden, F. G.; Gao, G. F. A novel coronavirus outbreak of global health concern. *Lancet.* **2020**, *395*, 470–473.

[2] Zhu, N.; Zhang, D. Y.; Wang, W. L.; Li, X. W.; Yang, B.; Song, J. D.; Zhao, X.; Huang, B. Y.; Shi, W. F.; Lu, R. J. et al. A novel coronavirus from patients with pneumonia in China, 2019. *N. Engl. J. Med.* **2020**, *382*, 727–733.

[3] World Health Organization. *Coronavirus Disease* (*COVID-19*) [Online]. https://www.who.int/emergencies/diseases/novel-coronavirus-2019 (accessed Feb, 2022).

[4] Huang, C. L.; Wang, Y. M.; Li, X. W.; Ren, L. L.; Zhao, J. P.; Hu, Y.; Zhang, L.; Fan, G. H.; Xu, J. Y.; Gu, X. Y. et al. Clinical features of patients infected with 2019 novel coronavirus in Wuhan, China. *Lancet* **2020**, *395*, 497–506.

[5] Hu, B.; Guo, H.; Zhou, P.; Shi, Z. L. Characteristics of SARS-CoV-2 and COVID-19. *Nat. Rev. Microbiol.* **2021**, *19*, 141–154.

[6] Corman, V. M.; Landt, O.; Kaiser, M.; Molenkamp, R.; Meijer, A.; Chu, D. K.; Bleicker, T.; Brunink, S.; Schneider, J.; Schmidt, M. L. et al. Detection of 2019 novel coronavirus (2019-nCoV) by real-time RT-PCR. *Euro Surveill.* **2020**, *25*, 2000045.

[7] Jin, Y. H.; Cai, L.; Cheng, Z. S.; Cheng, H.; Deng, T.; Fan, Y. P.; Fang, C.; Huang, D.; Huang, L. Q.; Huang, Q. et al. A rapid advice guideline for the diagnosis and treatment of 2019 novel coronavirus (2019-nCoV) infected pneumonia (standard version). *Mil. Med. Res.* **2020**, *7*, 4.

[8] Liu, G. Q.; Rusling, J. F. COVID-19 antibody tests and their limitations. *ACS Sens.* **2021**, *6*, 593–612.

[9] Gillot, C.; Douxfils, J.; Cadrobbi, J.; Laffineur, K.; Dogné, J. M.; Elsen, M.; Eucher, C.; Melchionda, S.; Modaffari, É.; Tré-Hardy, M. et al. An original ELISA-based multiplex method for the simultaneous detection of 5 SARS-CoV-2 IgG antibodies directed against different antigens. *J. Clin. Med.* **2020**, *9*, 3752.

[10] Frumence, E.; Lebeau, G.; Viranaicken, W.; Dobi, A.; Vagner, D.; Lalarizo Rakoto, M.; Sandenon Seteyen, A. L.; Giry, C.; Septembre-Malaterre, A.; Raffray, L. et al. Robust and low-cost ELISA based on IgG-Fc tagged recombinant proteins to screen for anti-SARS-CoV-2 antibodies. *J. Immunol. Methods* **2021**, *495*, 113082.

[11] Tan, C. W.; Chia, W. N.; Qin, X. J.; Liu, P.; Chen, M. I. C.; Tiu, C.; Hu, Z. L.; Chen, V. C. W.; Young, B. E.; Sia, W. R. et al. A SARS-CoV-2 surrogate virus neutralization test based on antibody-mediated blockage of ACE2-spike protein–protein interaction. *Nat. Biotechnol.* **2020**, *38*, 1073–1078.

[12] Soleimani, R.; Khourssaji, M.; Gruson, D.; Rodriguez-Villalobos, H.; Berghmans, M.; Belkhir, L.; Yombi, J. C.; Kabamba-Mukadi, B. Clinical usefulness of fully automated chemiluminescent immunoassay for quantitative antibody measurements in COVID-19 patients. *J. Med. Virol.* **2021**, *93*, 1465–1477.

[13] Infantino, M.; Grossi, V.; Lari, B.; Bambi, R.; Perri, A.; Manneschi, M.; Terenzi, G.; Liotti, I.; Ciotta, G.; Taddei, C. et al. Diagnostic accuracy of an automated chemiluminescent immunoassay for anti-SARS-CoV-2 IgM and IgG antibodies: An Italian experience. *J. Med. Virol.* **2020**, *92*, 1671–1675.

[14] Padoan, A.; Cosma, C.; Sciacovelli, L.; Faggian, D.; Plebani, M. Analytical performances of a chemiluminescence immunoassay for SARS-CoV-2 IgM/IgG and antibody kinetics. *Clin. Chem. Lab. Med.* **2020**, *58*, 1081–1088.

[15] Zhang, C.; Zheng, T. T.; Wang, H.; Chen, W.; Huang, X. Y.; Liang, J. Q.; Qiu, L. P.; Han, D.; Tan. W. H. Rapid one-pot detection of SARS-CoV-2 based on a lateral flow assay in clinical samples. *Anal. Chem.* **2021**, *93*, 3325–3330.

[16] Chen, R.; Ren, C. P.; Liu, M.; Ge, X. P.; Qu, M. S.; Zhou, X. B.; Liang, M. F.; Liu, Y.; Li, F. Y. Early detection of SARS-CoV-2 seroconversion in humans with aggregation-induced near-infrared emission nanoparticle-labeled lateral flow immunoassay. *ACS Nano* **2021**, *15*, 8996–9004.

[17] Wang, D. M.; He, S. G.; Wang, X. H.; Yan, Y. Q.; Liu, J. Z.; Wu, S. M.; Liu, S. G.; Lei, Y.; Chen, M.; Li, L. et al. Rapid lateral flow immunoassay for the fluorescence detection of SARS-CoV-2 RNA. *Nat. Biomed. Eng.* **2020**, *4*, 1150–1158.

[18] Wondfo, *2019-nCoV Antibody Test* (*Lateral Flow Method*) [online]. https://en.wondfo.com.cn/pt/index77.html (accessed Feb 1, 2022).

[19] Li, Z. T.; Yi, Y. X.; Luo, X. M.; Xiong, N.; Liu, Y.; Li, S. Q.; Sun, R. L.; Wang, Y. Q.; Hu, B. C.; Chen, W. et al. Development and clinical application of a rapid IgM-IgG combined antibody test for SARS-CoV-2 infection diagnosis. *J. Med. Virol.* **2020**, *92*, 1518–1524.

[20] Ravi, N.; Cortade, D. L.; Ng, E.; Wang, S. X. Diagnostics for SARS-CoV-2 detection: A comprehensive review of the FDA-EUA COVID-19 testing landscape. *Biosens. Bioelectron.* **2020**, *165*, 112454.

[21] Xu, L. Z.; Li, D. Y.; Ramadan, S.; Li, Y. B.; Klein, N. Facile biosensors for rapid detection of COVID-19. *Biosens. Bioelectron.* **2020**, *170*, 112673.

[22] Lou, B.; Li, T. D.; Zheng, S. F.; Su, Y. Y.; Li, Z. Y.; Liu, W.; Yu, F.; Ge, S. X.; Zou, Q. D.; Yuan, Q. et al. Serology characteristics of SARS-CoV-2 infection after exposure and post-symptom onset. *Eur. Respir. J.* **2020**, *56*, 2000763.

[23] Hou, H. Y.; Wang, T.; Zhang, B.; Luo, Y.; Mao, L.; Wang, F.; Wu, S. J.; Sun, Z. Y. Detection of IgM and IgG antibodies in patients with coronavirus disease 2019. *Clin. Transl. Immunol.* **2020**, *9*, e01136.

[24] Lauer, S. A.; Grantz, K. H.; Bi, Q. F.; Jones, F. K.; Zheng, Q. L.; Meredith, H. R.; Azman, A. S.; Reich, N. G.; Lessler, J. The incubation period of coronavirus disease 2019 (COVID-19) from publicly reported confirmed cases: Estimation and application. *Ann. Intern. Med.* **2020**, *172*, 577–582.

[25] Zhou, J.; Li, C.; Liu, X. J.; Chiu, M. C.; Zhao, X. Y.; Wang, D.; Wei, Y. X.; Lee, A.; Zhang, A. J.; Chu, H. et al. Infection of bat and human intestinal organoids by SARS-CoV-2. *Nat. Med.* **2020**, *26*, 1077–1083.

[26] Hui, K. P. Y.; Cheung, M. C.; Perera, R. A. P. M.; Ng, K. C.; Bui, C. H. T.; Ho, J. C. W.; Ng, M. M. T.; Kuok, D. I. T.; Shih, K. C.; Tsao, S. W. et al. Tropism, replication competence, and innate immune responses of the coronavirus SARS-CoV-2 in human respiratory tract and conjunctiva: An analysis in *ex-vivo* and *in-vitro* cultures. *Lancet Respir. Med.* **2020**, *8*, 687–695.

[27] World Health Organization. *Antigen-Detection in the Diagnosis of SARS-CoV-2 Infection* [Online]. https://www.who.int/publications/i/item/antigen-detection-in-the-diagnosis-of-sars-cov-2infection-using-rapid-immunoassays.

[28] Kim, H. Y.; Lee, J. H.; Kim, M. J.; Park, S. C.; Choi, M.; Lee, W.; Ku, K. B.; Kim, B. T.; Changkyun Park, E.; Kim, H. G. et al. Development of a SARS-CoV-2-specific biosensor for antigen detection using scFv-Fc fusion proteins. *Biosens. Bioelectron.* **2021**, *175*, 112868.

[29] Lee, J. H.; Choi, M.; Jung, Y.; Lee, S. K.; Lee, C. S.; Kim, J.; Kim, J.; Kim, N. H.; Kim, B. T.; Kim. H. G. A novel rapid detection for SARS-CoV-2 spike 1 antigens using human angiotensin converting enzyme 2 (ACE2). *Biosens. Bioelectron.* **2021**, *171*, 112715.

[30] Zhang, L. Y.; Fang, X. N.; Liu, X. B.; Ou, H. C.; Zhang, H. Y.; Wang, J. J.; Li, Q.; Cheng, H. Y.; Zhang, W. Y.; Luo, Z. F. Discovery of sandwich type COVID-19 nucleocapsid protein DNA aptamers. *Chem. Commun.* **2020**, *56*, 10235–10238.

[31] Lin, Q. Y.; Wen, D. H.; Wu, J.; Liu, L. L.; Wu, W. J.; Fang, X. E.; Kong, J. L. Microfluidic immunoassays for sensitive and simultaneous detection of IgG/IgM/antigen of SARS-CoV-2 within 15 min. *Anal. Chem.* **2020**, *92*, 9454–9458.

[32] Guo, J. C.; Chen, S. Q.; Tian, S. L.; Liu, K.; Ni, J.; Zhao, M.; Kang, Y. J.; Ma, X.; Guo, J. H. 5G-enabled ultra-sensitive fluorescence sensor for proactive prognosis of COVID-19. *Biosens. Bioelectron.* **2021**, *181*, 113160.

[33] Grant, B. D.; Anderson, C. E.; Williford, J. R.; Alonzo, L. F.; Glukhova, V. A.; Boyle, D. S.; Weigl, B. H.; Nichols, K. P. SARS-CoV-2 coronavirus nucleocapsid antigen-detecting half-strip lateral flow assay toward the development of point of care tests using commercially available reagents. *Anal. Chem.* **2020**, *92*, 11305–11309.

[34] Liu, D.; Ju, C. H.; Han, C.; Shi, R.; Chen, X. H.; Duan, D. M.; Yan, J. H.; Yan, X. Y. Nanozyme chemiluminescence paper test for rapid and sensitive detection of SARS-CoV-2 antigen. *Biosens. Bioelectron.* **2021**, *173*, 112817.

[35] Antaris, A. L.; Chen, H.; Cheng, K.; Sun, Y.; Hong, G. S.; Qu, C. R.; Diao, S.; Deng, Z. X.; Hu, X. M.; Zhang, B. et al. A small-molecule dye for NIR-II imaging. *Nat. Mater.* **2016**, *15*, 235–242.

[36] Hong, G. S.; Diao, S.; Chang, J. L.; Antaris, A. L.; Chen, C. X.; Zhang, B.; Zhao, S.; Atochin, D. N.; Huang, P. L.; Andreasson, K. I. et al. Through-skull fluorescence imaging of the brain in a new nearinfrared window. *Nat. Photonics* **2014**, *8*, 723–730.

[37] Welsher, K.; Liu, Z.; Sherlock, S. P.; Robinson, J. T.; Chen, Z.; Daranciang, D.; Dai, H. J. A route to brightly fluorescent carbon nanotubes for near-infrared imaging in mice. *Nat. Nanotechnol.* **2009**, *4*, 773–780.

[38] Kenry; Duan, Y. K.; Liu, B. Recent advances of optical imaging in the second near-infrared window. *Adv. Mater.* **2018**, *30*, 1802394.

[39] Chang, B. S. ; Li, D. F. ; Ren, Y. ; Qu, C. R. ; Shi, X. J. ; Liu, R. Q. ; Liu, H. G. ; Tian, J. ; Hu, Z. H. ; Sun, T. L. et al. A phosphorescent probe for *in vivo* imaging in the second near-infrared window. *Nat. Biomed. Eng.*, in press, https://doi.org/10.1038/s41551-021-00773-2.

[40] Zhu, S. J.; Tian, R.; Antaris, A. L.; Chen, X. Y.; Dai, H. J. Near-infrared-II molecular dyes for cancer imaging and surgery. *Adv. Mater.* **2019**, *31*, e1900321.

[41] Hong, G. S.; Lee, J. C.; Robinson, J. T.; Raaz, U.; Xie, L. M.; Huang, N. F.; Cooke, J. P.; Dai, H. J. Multifunctional *in vivo* vascular imaging using near-infrared II fluorescence. *Nat. Med.* **2012**, *18*, 1841–1846.

[42] Zhang, C. Y.; Zhou, L.; Du, K.; Zhang, Y.; Wang, J.; Chen, L. J.; Lyu, Y. N.; Li, J.; Liu, H.; Huo, J. L. et al. Foundation and clinical evaluation of a new method for detecting SARS-CoV-2 antigen by fluorescent microsphere immunochromatography. *Front. Cell Infect. Microbiol.* **2020**, *10*, 553837.

[43] Wang, C. W.; Yang, X. S.; Zheng, S.; Cheng, X. D.; Xiao, R.; Li, Q. J.; Wang, W. Q.; Liu, X. X.; Wang, S. Q. Development of an ultrasensitive fluorescent immunochromatographic assay based on multilayer quantum dot nanobead for simultaneous detection of SARS-CoV-2 antigen and influenza a virus. *Sens. Actuators B Chem.* **2021**, *345*, 130372.